



Research article

Magnetic molecularly imprinted polymers using ternary deep eutectic solvent as novel functional monomer for hydroxytyrosol separation

Xiaojing Wang^{a,1}, Mengru Wang^a, Bailin Wu^a, Shengyuan Yu^a, Zaizhi Liu^b, Xuyang Qin^a, Huijuan Xu^{a,1}, Wei Li^a, Sha Luo^a, Lijuan Wang^a, Chunhui Ma^{a,*}, Shouxin Liu^{a,**}

^a Key Laboratory of Bio-based Material Science and Technology (Ministry of Education), College of Material Science and Engineering, Northeast Forestry University, 150040, Harbin, China

^b College of Life Sciences, Jiangxi Normal University, 330022, Nanchang, China

ARTICLE INFO

Keywords:

Magnetic
Molecularly imprinting polymers (MIPs)
Deep eutectic solvent (DES)
Hydroxytyrosol (HT)

ABSTRACT

In this work, magnetic molecularly imprinted polymers (MIPs) for specific recognition of Hydroxytyrosol (HT) were designed by vinyl-modified magnetic particles ($\text{Fe}_3\text{O}_4@ \text{SiO}_2@ \text{VTEOs}$) as carrier, ternary deep eutectic solvent (DES) as functional monomer, while ethylene glycol dimethacrylate (EGDMA) as crosslinker. The optimum amount of DES was obtained by adsorption experiments (molar ratio, caffeic acid: choline chloride: formic acid = 1:6:3) which were 140 μL in total. Under the optimized amount of DES, the maximum adsorption capacity of the MIPs particles was 42.43 mg g^{-1} , which was superior to non-imprinted polymer (4.64 mg g^{-1}) and the imprinting factor (IF) is 9.10. Syringin and Oleuropicrin were used as two reference molecules to test the selectivity of the DES-MIPs particles. The adsorption capacity of HT was 40.11 mg g^{-1} . Three repeated experiments show that the polymer has high stability and repeatability (RSD = 5.50).

1. Introduction

Hydroxytyrosol (HT) is a natural polyphenolic compound with strong antioxidant and mainly exists in the form of esters in olive fruits and branches and leaves [1]. HT has been extensively studied for its various active effects, such as strong oxidation [2,3], anti-inflammatory [4–6], antibacterial [7], etc. HT can also prevent and cure lung cancer, occult breast cancer, uterine cervical cancer, hormone refractory prostate cancer, etc., promote cancer-later recovery and improve the effect of chemotherapy, because of its free hydroxyl, which has strong anti-cancer properties [8]. There have been many studies on the pharmacological effects of HT in anti-cancer [9], anti-thrombosis [10], anti-arteriosclerosis [11], prevention and treatment of macular degeneration [12], protection of

* Corresponding author. Key Laboratory of Bio-based Material Science and Technology (Ministry of Education), College of Material Science and Engineering, Northeast Forestry University, Harbin, 150040, China.

** Corresponding author. Key Laboratory of Bio-based Material Science and Technology (Ministry of Education), College of Material Science and Engineering, Northeast Forestry University, Harbin, 150040, China.

E-mail addresses: mchmchmchmch@163.com (C. Ma), liushouxin@126.com (S. Liu).

¹ These authors are equal to this research work.

<https://doi.org/10.1016/j.heliyon.2024.e28257>

Received 1 August 2023; Received in revised form 14 March 2024; Accepted 14 March 2024

Available online 15 April 2024

2405-8440/© 2024 The Authors. Published by Elsevier Ltd. This is an open access article under the CC BY-NC license (<http://creativecommons.org/licenses/by-nc/4.0/>).

cartilage [13] and other aspects, and also discussed the pharmacological mechanism of HT. However, the yield of HT extracted from olive products is low [14], which because it exists in esters-Oleuropein form. Furthermore, the hydrolysis reaction conditions catalyzed by inorganic acids and bases were complex, and also lead to low HT yield and environmental pollution [15]. We hoped to extract HT specifically from *Syringa oblata Lindl.*, but lilac extract contains not only HT, but also Syringin and Oleuropein.

Molecular Imprinting Technology with many irreplaceable advantages was applied in the natural products separation field. The target molecules were captured and bound within the specific recognition sites designed in the molecularly imprinted polymers (MIPs). And then were eluted by a suitable solvent to obtain the target compounds of high purity [16]. MIPs have the advantages of high affinity and selectivity, strong resistance to adverse environment, good stability, and long service life [17]. The selectivity, durability and repeatability of the design molecules have made these polymers a focus for scientists [18]. For example, MIPs can be used to separate flavonoids from ginkgo biloba leaves [18], simultaneously determine a variety of phenolic compounds from water [19], identify alkaloids from water [20], and remove cholesterol from milk [21].

The crisis of the ecological environment calling for green chemistry. In recent years, deep eutectic solvents (DESs) have been applied widely in molecular imprinting technology as a result of its advantages of excellent solubility, solvent recovery, low toxicity and easy degradation [22–24]. DES consists of a hydrogen bond donor (HBD), which is usually an Alcohols, sugars or organic acids, and a hydrogen bond acceptor (HBA), which is halides (choline chloride) or organic salt. The formation conditions are mainly temperature and mechanical agitation, and the final state is stable and uniform transparent liquid [25]. As an imprinting technique, molecular imprinting technology also has the ability to synthesize polymers on the surface of the substrate using solid materials to improve the recognition efficiency of polymers [26]. Fe_3O_4 is used as a matrix because of its magnetism [27]. However, Fe_3O_4 is easy to agglomerate in dispersion solution, so the aggregation effect can be weakened by adding modification layer on the surface [28–30]. As a functional monomer of MIPs, DES is better than the normal functional monomer synthesized MIPs. DES-MIPs has better specific recognition and selective recognition advantages for samples, and has higher stability of imprinting factors [31–33], which indicates that the research on integrating DES into MIP has development potential. Unfortunately, the high viscosity of binary DES leads to serious adhesion of synthesized DES-MIPs resulting in low specific surface area causing lower adsorption performance [34]. As a result, multiple (ternary) DES is proposed to be introduced into the preparation of polymer as a functional monomer.

In this paper, ternary DES, which was synthesized from choline chloride (ChCl), caffeic acid (CA) and formic acid (FA), was introduced as functional monomer to prepare MIPs (DES-MIPs) to achieve specific adsorption separation of target HT. For rapid magnetic separation, DES-MIPs was prepared by using modified magnetic $\text{Fe}_3\text{O}_4@SiO_2@VTEOs$ nanoparticles as the matrix. The morphology, structure, weight ratio, chemical bond, magnetism, and particle size of DES-MIPs were analyzed by characterization. Furthermore, the binding experiment, selectivity and repeatability test of DES-MIPs are systematically discussed.

2. Materials and methods

2.1. Chemical reagents

Hydroxytyrosol (HT, HPLC \geq 98 %, CAS: 10597-60-1) was purchased from Xinyang Zhongjian Metrological Biotechnology Co., Ltd (Henan, China), Oleuropein(HPLC \geq 98 %, CAS: 32619-42-4), Syringin (HPLC \geq 98 %, CAS: 118-34-3) were purchased from Chemical Purity of Plant Standard Co., Ltd. (chengdu, China).Choline Chloride (ChCl, AR, \geq 98 %, CAS: 67-48-1), 2,2- azobisisobutyronitrile (AIBN, AR, \geq 98 %, CAS: 78-67-1),caffeic acid (CA, AR, \geq 98 %, CAS: 331-39-5), Formic acid (FA, AR, \geq 98 %, CAS: 64-18-6), ethylene glycol dimethacrylate (EGDMA, AR, 98 %, CAS: 97-90-5) and Triethoxyvinylsilan (VTEOs, AR, 97 %, CAS: 78-08-0) were purchased from Macklin Biochemical Co., Ltd (Shanghai, China). Ammonium hydroxide solution ($\text{NH}_3\cdot\text{H}_2\text{O}$, GR, CAS: 1336-21-6), Tetraethyl orthosilicate (TEOs, AR, 98 %, CAS: 78-10-4), Acetic Acid (AC, AR, 99.8 %, CAS: 64-19-7) and Acetonitrile (ACN, AR, 99.5 %, CAS: 75-05-8) were purchased from Kermel (Tianjin, China). Ethanol absolute (AR, 99.7 %, CAS: 141-78-6) were purchased from Tianli Chemical Reagent Co., Ltd. (Tianjin, China).

2.2. Characterization methods

The surface morphology of polymers was observed by Tescan MIRA LMS scanning electron microscope (SEM) (Tescan China, China). The core-shell structure of $\text{Fe}_3\text{O}_4@SiO_2@VTEOs$ was characterized by Tecnai G2 F30 S-TWIN transmission electron microscopy (TEM) (FEI, USA). The particle size was determined using a dynamic light scattering (DLS) of NanoBrook Omni (Brookhaven, USA). FT-IR spectra were recorded by a spectrometer with the model of iS10 (Nicolet, USA). The D8 Advance ray diffractometer (BRUKER, Germany) was used to analyze the crystallinity of Fe_3O_4 . Thermal gravimetric analysis (TGA) was measured to explore the thermal weightlessness of samples by a DSC1/1600LF thermal gravimetric analyzer (METTLER TOLEDO, Swiss Confederation). Furthermore, the vibrating sample magnetometer (VSM) with a MPMS-3 (Quantum Design, USA) was used to analyzed magnetization of polymers.

2.3. Preparation of ternary DES

Ternary DES (CA-ChCl-FA, molar ratio 1:6:3) were prepared by heating method, that is, stirred at 80 °C until a uniform and transparent liquid was obtained [35]. Then collect the ternary DES for use.

2.4. Preparation method of Fe₃O₄@SiO₂@VTEOs

To remove impurities on the surface of Fe₃O₄, 4.00 g Fe₃O₄ nanoparticles were introduced to 400 mL deionized water-ethanol (1:1, v/v) solution, which were dispersed under ultrasound for 25 min prior to being separated by magnetic field. Dried by vacuum-drying at 40 °C.

To prepare Fe₃O₄@SiO₂ nanoparticles, 1.00 g treated Fe₃O₄ nanoparticles were added to 200 mL of Ethanol absolute and dispersed under ultrasonic action for 10 min. Afterwards, 10 mL of NH₃·H₂O and 0.50 mL of Tetraethyl orthosilicate (TEOs) were introduced to the mixture and reacted 2 h at ambient temperature under mechanical stirring. Add 1.0 mL TEOs to the mixture and the reaction lasted 3 h. The synthesized Fe₃O₄@SiO₂ nanoparticles were rinsed thoroughly with deionized water, repeating the washing process 5–6 times until the solution reached a neutral pH level. Products were dried by vacuum-drying at 40 °C.

To modified Fe₃O₄@SiO₂ nanoparticles by Triethoxyvinylsilan (VTEOs), 0.50 g of prepared Fe₃O₄@SiO₂ were introduced to 30 mL of 10 % ethanol solution, dispersing for 10 min before adding 3.0 mL of VTEOs. After that, the mixture was mechanically stirred for 5 h at 50 °C. The Fe₃O₄@SiO₂@ Triethoxyvinylsilan (Fe₃O₄@SiO₂@VTEOs) nanoparticles were washed with deionized water 6–7 times. Then the particles were separated by magnetic field. Afterwards, Fe₃O₄@SiO₂@VTEOs were dried by vacuum-drying at 40 °C.

2.5. Preparation method of ternary DES-MIPs

Mixed 70.0 mg Fe₃O₄@SiO₂@VTEOs with 30 mL acetonitrile solution for 10 min by sonication. After that, 0.1 mmol (13.9 mg) of HT and 140 μL DES were dissolved in the above solution, dispersing for 10 min. The reaction was pre-assembly for 3 h at 50 °C in water bath oscillator. Then, 5 mmol (1.0 mL) of EGDMA as cross linker was added in the mixtures, and the reaction system was charged with nitrogen for 13 min before the system was quickly shut down by the addition of 0.12 mmol (20.0 mg) of AIBN as an initiator. The polymerization was then carried out in a water-bath shaker at 60 °C for 12 h. The fabricated particles were separated using magnet field, then they were washed with methanol-acetic acid (9:1, v/v) to remove template molecule (HT). After multiple elution operations, the elution fluid was detected by HPLC. If there was no HT in the detection solution, the preparation of DES-MIP was successful. Except for not adding HT, DES-NIP was prepared in the same way (n ≥ 3).

2.6. HPLC detection method of HT

HPLC analysis was accomplished with a 1260–6420 Triple Quad LC/MS (Agilent, USA). The SB-C18 column (4.6 mm × 150, 5 μm, Agilent Technologies, USA) was used as the chromatographic column. The mobile phase was composed of methanol (solvent A) and 0.1 % aqueous formic acid (solvent B). The duration of analysis was 19 min at isocratic conditions when mobile phase composition was 37 % of A and 63 % of B. The temperature of the column was maintained at 25 °C and the injection volume was set to 0.5 μL. The detection wavelength was 280 nm.

2.7. Static adsorption experiments

2.7.1. Adsorption and desorption kinetics experiment

Adsorption kinetics experiment was actualized for assessment of adsorption efficiency of HT on MIPs. 4.0 mg DES-MIPs and DES-NIPs were dispersed in 1.0 mL of 1.0 mg/mL HT methanol solution respectively. Oscillate at 150 rpm in a 25 °C vibrator for varying amounts of time (0–360 min). Subsequently, DES-MIPs and DES-NIPs were separated and the filtrates were obtained and detected by HPLC. The adsorption capacity (Q, mg/g) of HT on DES-MIPs and DES-NIPs was calculated according to Eq. (1):

$$Q = \frac{(C_0 - C_s) \times V}{M} \quad (1)$$

Q (mg/g) was the adsorption capacity of polymers for HT. C₀ was concentration of HT in solution before adsorbed by polymers and C_s (mg/mL) was concentration of HT after being adsorbed. In addition, V (mL) was the volume of HT solution, and M (g) was the weight of polymers.

The recognition performance of DES-MIPs for HT was estimated by the imprint factor (IF), which was calculated as Eq. (2):

$$IF = \frac{Q_m}{Q_n} \quad (2)$$

Q_m (mg g⁻¹) and Q_n (mg g⁻¹) were the adsorbed HT on DES-MIPs and DES-NIPs.

Desorption experiments were also done for the highest adsorbed number of DES-MIPs. The eluent was methanol-acetic acid solution (v:v = 9:1), which was oscillated at 150 rpm in a 25 °C vibrator for different time (0–120 min). Subsequently, DES-MIPs and DES-NIPs were separated and the filtrates were obtained and detected by HPLC. The desorption capacity (Q, mg/g) of HT on DES-MIPs was calculated according to Eq. (3):

$$Q = \frac{C_d \times V}{M} \quad (3)$$

Here Q (mg/g) was the desorption capacity of HT on DES-MIPs. C_d (mg/mL) was concentration of HT after being desorbed. In addition, V (mL) was the volume of HT solution and M (g) was the weight of DES-MIPs or DES-NIPs.

2.7.2. Effect of DES dosage on adsorption capacity

The novelty of this experiment lies in the use of DES as a functional monomer to synthesize MIPs. In order to research the effect of DES amount on adsorption performance, MIPs and NIPs were synthesized using the amount of DES as a variable (100 μ L–180 μ L). Other experiments and analysis procedures were the same as adsorption kinetics experiments. The synthesis designation with different amount of DES was shown in Table S1.

2.7.3. Adsorption isotherm experiment

Adsorption isotherm was used to judge and obtain the adsorption capacity of DES-MIPs. 4.0 mg of DES-MIPs and DES-NIPs were added into 1.0 mL of HT methanol solution (concentrations ranging from 0.2 mg/mL to 1.2 mg/mL), respectively. Oscillate for 300 min at 150 rpm in a 25 °C vibrator. The analysis process of this part of the experiment is the same as the above dynamic experiment.

2.7.4. Selectivity experiment

A selectivity experiment was carried out to assess the specific recognition performance of DES-MIPs for HT. Because lilac extract contains not only HT, but also Oleuropein and Syringin. Oleuropein and Syringin were introduced as the competitor of HT. 4.0 mg of DES-MIPs and DES-NIPs were added to 1.0 mL of a methanol mixture of HT, Oleuropein and Syringin (1.0 mg/mL), respectively. Oscillate for 300 min at 150 rpm in a 25 °C vibrator. After adsorption equilibrium, DES-MIPs and DES-NIPs were separated and the filtrates were obtained and detected by HPLC. It can be seen from Fig. 1, the retention time of HT, Syringin and Oleuropein were 8.853 min, 13.733 min, and 33.04 min respectively.

2.7.5. Reusability experiment

To evaluate the practical application possibility and value of DES-MIPs, and to study its stability and repeatability so as to design repeatability experiments. Dispersing 4.0 mg DES-MIPs and DES-NIPs in 1.0 mL of 1.0 mg/mL HT methanol solution. Oscillate for 300 min at 150 rpm in a 25 °C vibrator. HT was eluted with methanol-acetic acid (9:1, v/v) as the eluting solvent. The adsorption/ desorption cycle was performed 3 times.

3. Results and discussion

3.1. Preparation of MIPs

DES-MIPs was synthesized as follows. First, the Fe₃O₄ nanoparticles are ultrasonic cleaned with an aqueous ethanol solution to remove surface impurities. Fe₃O₄ nanoparticles are easy to agglomerate and precipitate in dispersion solution. The Fe₃O₄ particles dispersed in the solution are unstable and prone to oxidation, resulting in the loss of their magnetic properties. In this case, Fe₃O₄ nanoparticles were modified by a self-assembly layer-by-layer polymerization. Fe₃O₄ nanoparticles coated with non-polar materials can improve their stability, dispersibility and avoid agglomeration of Fe₃O₄ nanoparticles. Because the SiO₂ can form a hollow shell on the surface of Fe₃O₄ to improve the hydrophobicity of Fe₃O₄, but the addition of SiO₂ will reduce the magnetism of Fe₃O₄ per unit mass, which will make the MIP separation difficult [36–39]. In addition, silica has good biocompatibility, hydrophilicity, and easy functionalization. and then Fe₃O₄@SiO₂ nanoparticles were modified by VTEOs to reduce the agglomeration between matrix particles and enhance the binding force with functional monomers and template molecules. It is then functionalized by a simple reaction between the Si–O bond on the surface of Fe₃O₄@SiO₂ particles and the vinyl group of VTEOs. Grafting of VTEOs onto Fe₃O₄@SiO₂ surface to form functionalized Fe₃O₄@SiO₂@VTEOs particles.

In the synthesis process, DES, EGDMA, HT, AIBN and Fe₃O₄@SiO₂@VTEOs nanoparticles as functional monomer, crosslinking

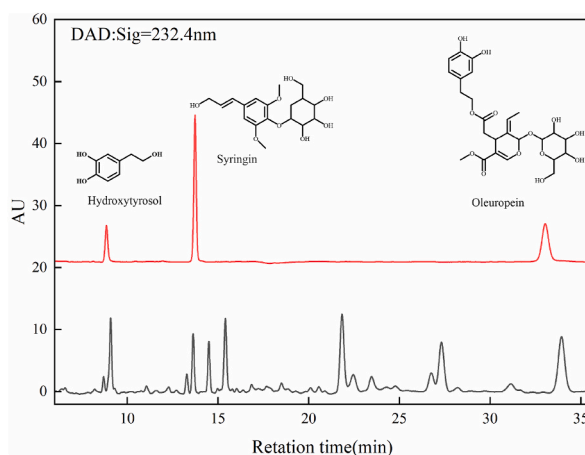


Fig. 1. HPLC of samples and standards (syringin, oleuropein and hydroxytyrosol).

agent, template, initiator and magnetic provider, respectively. magnetic provider. In this experiment, the novelty of MIPs lies in the application of ternary DES in the preparation. Molecular imprinting is accomplished by (1) covalent or π and non-covalent bonds between imprinted molecules and functional monomer to form Host-guest complex. (2) crosslinker was added into the complex, which was initiated by initiator, and the imprinted molecule-monomer complex was polymerized. In this process, the template and monomer complexes are “Trapped” into the stereo structure of the MIP by radical polymerization. (3) the template in the MIP is removed by appropriate solvent elution or dissociation to form binding sites with recognition of the imprinted molecules. Firstly, in our research, the main function of the functional monomers is to immobilize template molecules through hydrogen bonding (non-covalent bonds).

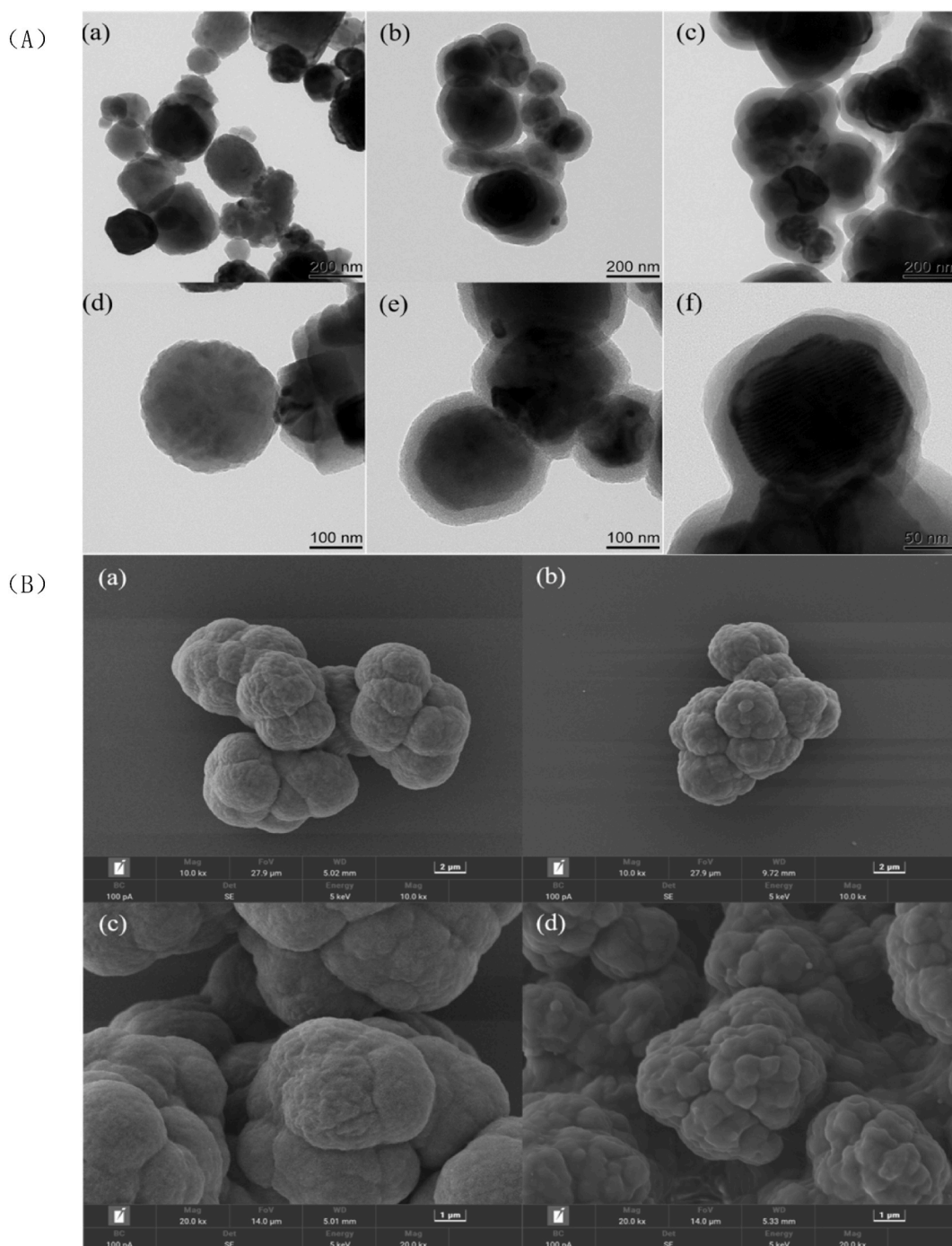


Fig. 2. TEM images (A) of Fe₃O₄ (a and d), Fe₃O₄@SiO₂ (b and e), Fe₃O₄@SiO₂@VTEOs (c and f), and SEM images (B) of DES-MIPs (a and c) and DES-NIPs (b and d).

Obviously, as a polyhydroxy compound, caffeic acid can form more hydrogen bonds with template molecules. Secondly, the polymerization reaction needs to be carried out in a stable chemical solvent, and the low eutectic system formed by choline chloride and caffeic acid provides a good dissolution effect and chemical reaction environment for the reactants (including crosslinking agents and initiators). Finally, compared the polymerization efficiency of DESs with different composition, caffeic acid: choline chloride: formic acid = 1:6:3 (molar ratio) was determined as the optimum solvent composition. Choline chloride is a hydrogen-bonding receptor, caffeic acid and formic acid are hydrogen-bonding donors, forming a stable polyhydroxy eutectic system, not only as a reaction solvent system, and also as a functional monomer to immobilize template molecules through hydrogen bonds. Finally, DES-MIPs were successfully prepared by washing out the HT template molecules using a methanol-acetic acid (9:1, v/v) mixture as eluent (Table S2). When the eluent was methanol-acetic acid (9:1, v/v), HT can be recovered up to 45.54 mg.

3.2. Characteristics of DES-MIPs

3.2.1. TEM and SEM characterizations

To clearly observe morphological differences of the particle, Fe_3O_4 , $\text{Fe}_3\text{O}_4@SiO_2$ and $\text{Fe}_3\text{O}_4@SiO_2@VTEOs$ were measured by TEM, and the morphology and size of the three substances at the nanometer scale could be clearly observed in the TEM images. It can be seen in Fig. 2(A), $\text{Fe}_3\text{O}_4@SiO_2$ and $\text{Fe}_3\text{O}_4@SiO_2@VTEOs$ were spherical and covered by transparent materials, with increasing thickness. It can be observed by SEM in Fig. 2(B), which the surface morphology of DES-NIPs and DES-MIPs was similar, but the structure of NIPs was denser and smoother than that of MIP. Because of there were many pores on the surface of DES-MIPs, which were the reason for the specific adsorption of DES-MIPs.

3.2.2. DLS analysis of magnetic DES-MIPs

The particle size was analyzed according to the grain size distribution diagram (Fig. 3) derived from the dynamic light scattering (DLS) study. These particle size ranges for Fe_3O_4 (122–164 nm), $\text{Fe}_3\text{O}_4@SiO_2$ (295–396 nm), $\text{Fe}_3\text{O}_4@SiO_2@VTEOs$ (342–459 nm), and DES-MIPs (459–615 nm) can be seen in Table S3. All four kinds of particles were placed in ultrapure water and then ultrasonic for 30 min, which was observed to be larger than TEM test results, because the particle size measured by DLS was hydration particle size, which was the result of agglomeration of some particles. DLS experiment showed that Fe_3O_4 were successfully wrapped by SiO_2 and VTEOs.

3.2.3. FT-IR characterization of magnetic DES-MIPs

Fig. 4(a) showed the FT-IR spectra of polymers. The peak at 601 in curve 1 was the peak of the Fe–O stretching vibration. The peak at 1058 in curve 2 belongs to Si–O–Si characteristic peak, which can also be observed in curves 3 and 4. In comparison with curve 2, peaks at 1597 and 1409 appear in curve 3, where small and sharp absorption peaks indicated that the nanoparticles were equipped with unsaturated double bonds, and there were indeed unsaturated double bonds in VTEOs, so it proves that VTEOs was successfully wrapped on the surface of $\text{Fe}_3\text{O}_4@SiO_2$. It can be seen from curve 4 that the absorption peak of 1720 appeared in comparison curve 3, and the Si–O–Si characteristic peak weakened, indicating that the polymer was successfully wrapped by crosslinker, and the DES-MIP polymer was successfully prepared.

3.2.4. XRD analysis of magnetic DES-MIPs

The integrity of the Fe_3O_4 crystal structure during polymer synthesis was demonstrated by analyzing Fe_3O_4 , $\text{Fe}_3\text{O}_4@SiO_2$, $\text{Fe}_3\text{O}_4@SiO_2@VTEOs$ and DES-MIPs by X-ray diffractometer. From Fig. 4(b), it could be seen that the four substances showed distinct characteristic peaks at $2\theta = 30.3^\circ$, 35.6° , 43.4° , 54.5° , 57.4° and 62.9° . The opposite diffraction of these six peaks occurred at (220), (311), (400), (422), (511) and (440), respectively. This indicates that after many times modification experiments, the signals of $\text{Fe}_3\text{O}_4@SiO_2$, $\text{Fe}_3\text{O}_4@SiO_2@VTEOs$ and DES-MIPs were consistent with Fe_3O_4 particles. The results showed that crystal structure of

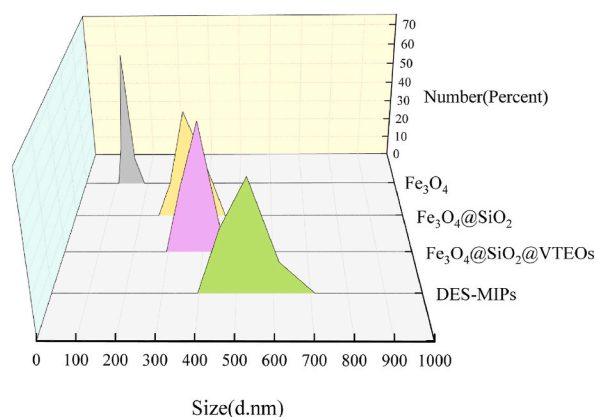


Fig. 3. DLS analysis of Fe_3O_4 , $\text{Fe}_3\text{O}_4@SiO_2$, $\text{Fe}_3\text{O}_4@SiO_2@VTEOs$ and DES-MIPs.

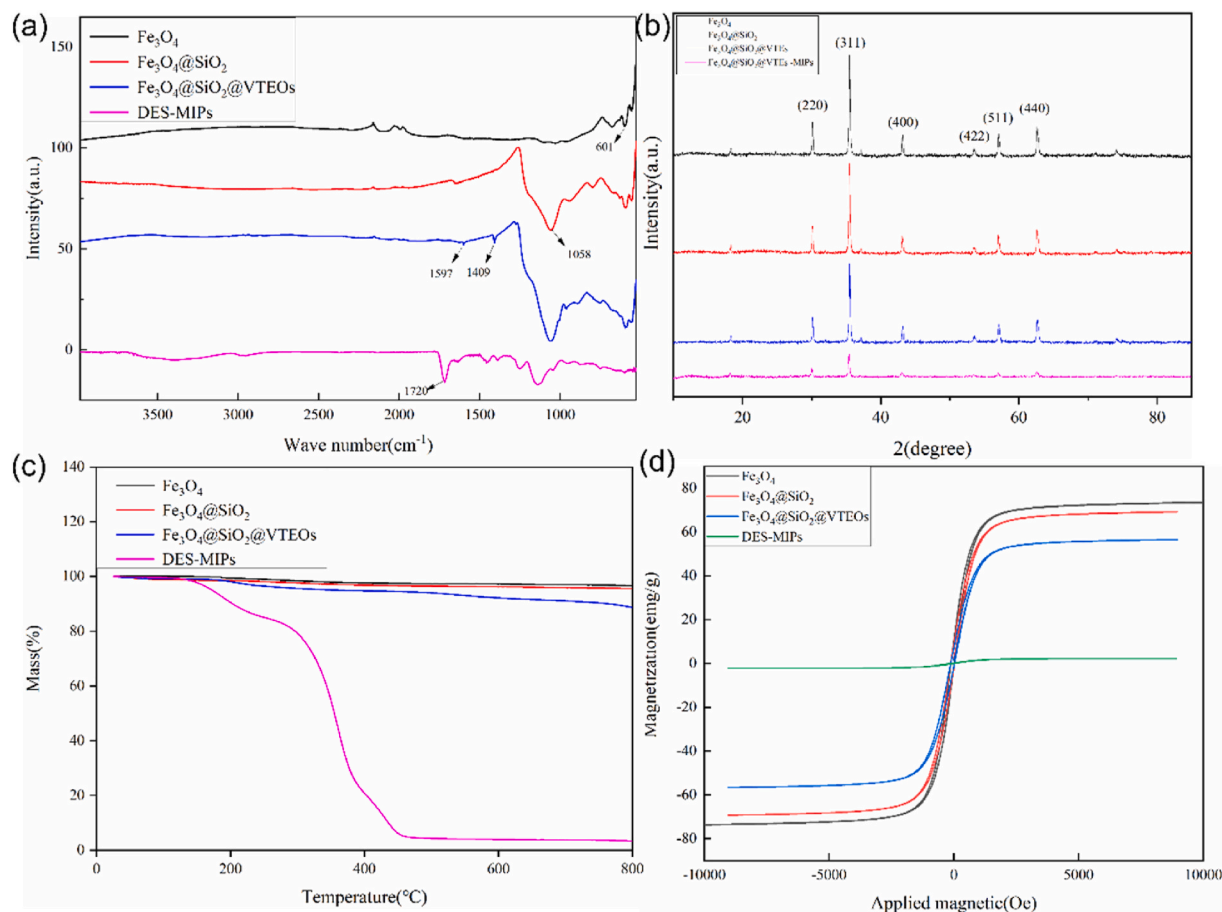


Fig. 4. Characterizations of Fe_3O_4 , $\text{Fe}_3\text{O}_4@SiO_2$, $\text{Fe}_3\text{O}_4@SiO_2@VTEOs$ and magnetic DES-MIPs (a) FT-IR spectra of Fe_3O_4 , $\text{Fe}_3\text{O}_4@SiO_2$, $\text{Fe}_3\text{O}_4@SiO_2@VTEOs$ and magnetic DES-MIPs (b) X-ray diffractometer of Fe_3O_4 , $\text{Fe}_3\text{O}_4@SiO_2$, $\text{Fe}_3\text{O}_4@SiO_2@VTEOs$ and magnetic DES-MIPs (c) TGA curves of Fe_3O_4 , $\text{Fe}_3\text{O}_4@SiO_2$, $\text{Fe}_3\text{O}_4@SiO_2@VTEOs$ and magnetic DES-MIPs (d) Magnetic hysteresis loops of Fe_3O_4 , $\text{Fe}_3\text{O}_4@SiO_2$, $\text{Fe}_3\text{O}_4@SiO_2@VTEOs$ and magnetic DES-MIPs to external magnetic field.

Fe_3O_4 sphere was not suffered a destruction the synthesis of polymer.

3.2.5. TGA analysis magnetic DES-MIPs

In order to evaluate the weight ratio of coating on Fe_3O_4 particles, Fe_3O_4 , $\text{Fe}_3\text{O}_4@SiO_2$, $\text{Fe}_3\text{O}_4@SiO_2@VTEOs$ and DES-MIPs were characterized using TGA, and the related results were shown in Fig. 4(c), the mass loss from 30 to 200 °C was caused by the vaporization of H_2O . The weight loss of the four substances at this temperature range were 0.606 %, 1.503 %, 1.886 % and 9.47 % respectively. As the temperature continues to increase, the weight loss of Fe_3O_4 and $\text{Fe}_3\text{O}_4@SiO_2$ was not great, by 800 °C, the weight loss was 3.357 % and 4.40 %, respectively. At 800 °C, the loss of $\text{Fe}_3\text{O}_4@SiO_2@VTEOs$ particles was 11.33 %. For DES-MIPs, the loss was 84.28 % at 200–450 °C and 96.59 % at 800 °C. It was because the polymer pore structure was too rich, the temperature too high caused by thermal cracking. DES-MIPs have excellent thermal stability below 150 °C. It further indicated that DES-MIPs was successful.

3.2.6. VSM analysis of magnetic DES-MIPs

Magnetic strength is a very important factor for magnetic materials. Magnetic properties of synthesized polymers were characterized by VSM, and magnetic hysteresis loops were shown in Fig. 4(d). The magnetic saturation strength of Fe_3O_4 , $\text{Fe}_3\text{O}_4@SiO_2$, $\text{Fe}_3\text{O}_4@SiO_2@VTEOs$, DES-MIPs were 73.65 emu/g, 69.19 emu/g, 56.52 emu/g and 2.22 emu/g. It can be found that the magnetic saturation intensity of $\text{Fe}_3\text{O}_4@SiO_2$, $\text{Fe}_3\text{O}_4@SiO_2@VTEOs$ and DES-MIPs was gradually weakening, and lower than that of Fe_3O_4 , because the material modified on the surface of Fe_3O_4 gradually thickens, its magnetic intensity gradually weaken. Although the magnetic intensity of DES-MIPs weaker than that of Fe_3O_4 , the magnetic saturation intensity of DES-MIPs is still sensitive to magnetic field, which was sufficient to realize the separation of polymer and solvent.

3.3. Static adsorption of HT on MIPs

3.3.1. Adsorption and desorption kinetics study

The adsorption efficiency of HT on DES-MIPs was verified by adsorption kinetics tests.

As can be seen from Fig. 5(a), the amount of HT adsorbed by DES-MIPs and DES-NIPs increased with time, and both reached adsorption equilibrium approximately 300 min. In addition, the adsorption capacity of DES-MIPs was significantly more than that of DES-NIPs.

To further understand interaction patterns between HT and DES-MIPs, kinetic data were evaluated using Pseudo-first order (4) and Pseudo-second order (5) models. The model equation was as follows:

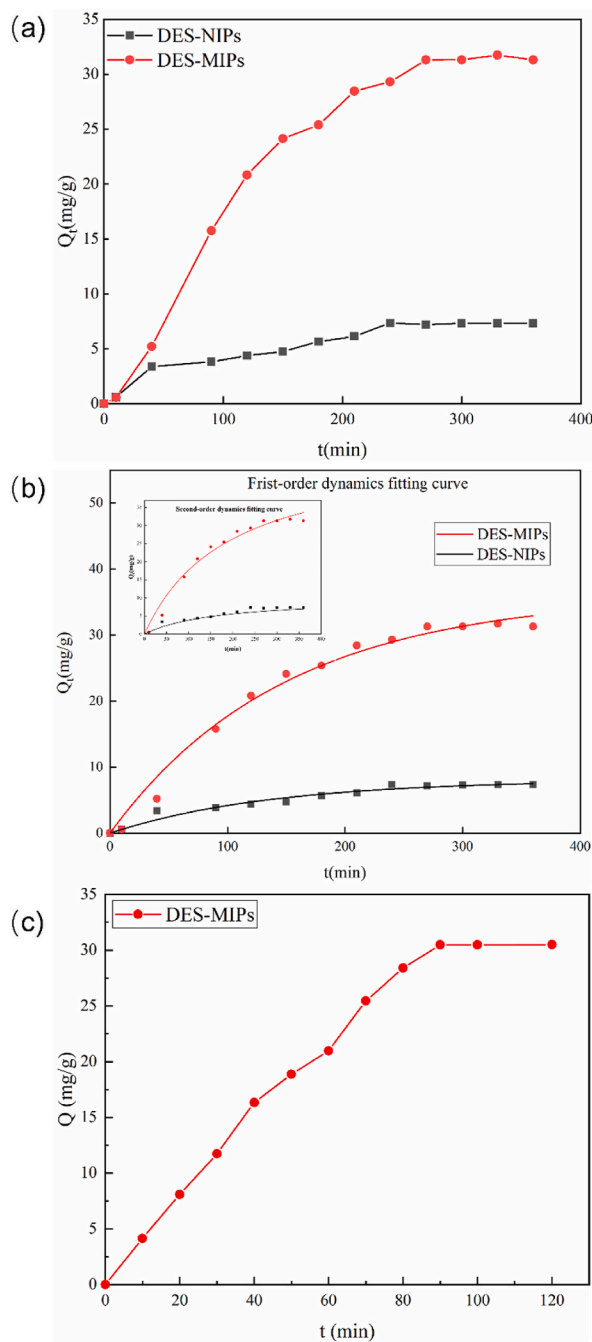


Fig. 5. Adsorption kinetic curves (a), Pseudo-first-order and Pseudo-second-order fitting curves (b) of DES-MIPs and DES-NIPs and Desorption kinetic curves (c).

Pseudo-first order (4):

$$\ln(Q_e - Q_t) = \ln Q_e - k_1 t \quad (4)$$

Pseudo-second order (5):

$$\frac{t}{Q_t} = \frac{1}{k_2 Q_e^2} + \frac{t}{Q_e} \quad (5)$$

Here k_1 (min^{-1}) and k_2 ($\text{g mg}^{-1} \text{min}^{-1}$) were the rate constants for the Pseudo-first order and Pseudo-second-order models, respectively. Q_e ($\text{mg}\cdot\text{g}^{-1}$) and Q_t ($\text{mg}\cdot\text{g}^{-1}$) were the adsorption capacities at equilibrium and at time t of adsorption of DES-MIPs and DES-NIPs to HT, respectively. t (min) was the time of adsorption.

In Fig. 5(b), adsorption mechanism was inferred by Pseudo-first order and Pseudo-second-order kinetic fitting model. For both DES-MIPs and DES-NIPs, the fitting degree of Eq. (4) (DES-MIPs: $R^2 > 0.98623$ and DES-NIPs: $R^2 > 0.95824$) was superior to that of Eq. (5) (DES-MIPs: $R^2 > 0.98007$ and DES-NIPs: $R^2 > 0.9163$). So, the Pseudo-first-order kinetic equation was applied to this adsorption experiment, and the adsorption process was mainly controlled by monolayer adsorption.

Experiments were carried out for the selection of the optimum desorption time. From Fig. 5(c), DES-MIPs have desorbed nearly all the HT at 90 min with a recovery of 97.31 %. So, the elution time of 90 min is optimal.

3.3.2. Effect of DES amount on HT adsorption

Static adsorption experiments were carried out on the synthesized DES-MIPs, and it was found that if DES dosage was different, IF was different, and DES-MIP3 showed the best adsorption performance. The optimal amount of DES was 140 μL . Fig. 6 showed the adsorption capacity of DES-MIPs.

3.3.3. Adsorption isotherm study

As can be seen in Fig. 7, the adsorption capacity of DES-MIPs for HT gradually increases as the initial concentration of HT increased. When the concentration of HT increased to 1.0 $\text{mg}\cdot\text{mL}^{-1}$, it was found that the adsorption capacity would not increase as the concentration continued to increase, so DES-MIPs reached adsorption saturation at the concentration of 1.0 $\text{mg}\cdot\text{mL}^{-1}$. Besides, the amount of HT adsorbed at adsorption equilibrium ($Q = 42.43 \text{ mg}\cdot\text{g}^{-1}$) was much greater than that of DES-NIPs ($Q = 4.67 \text{ mg}\cdot\text{g}^{-1}$). This indicated that DES-MIPs has specific recognition sites for HT, which makes DES-MIPs have excellent adsorption performance than DES-NIPs.

Thermodynamic fitting according to Langmuir equation (6):

$$\frac{C_e}{Q_e} = \frac{1}{Q_{\max} K_L} + \frac{C_e}{Q_{\max}} \quad (6)$$

Thermodynamic fitting according to Freundlich equation (7):

$$\ln Q_e = \ln k_F + \frac{1}{n} \ln C_e \quad (7)$$

Q_e (mg/g) is the experimental maximum adsorption capacity of the adsorbent for HT and Q_{\max} is the theoretical maximum adsorption capacity of the adsorbent for HT. C_e (mg/mL) represents analyte concentration at adsorption equilibrium and n is a constant

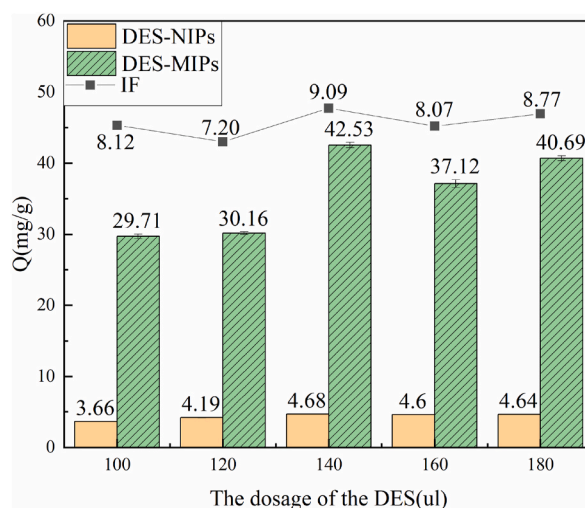


Fig. 6. Effect of different DES dosage on HT adsorption.

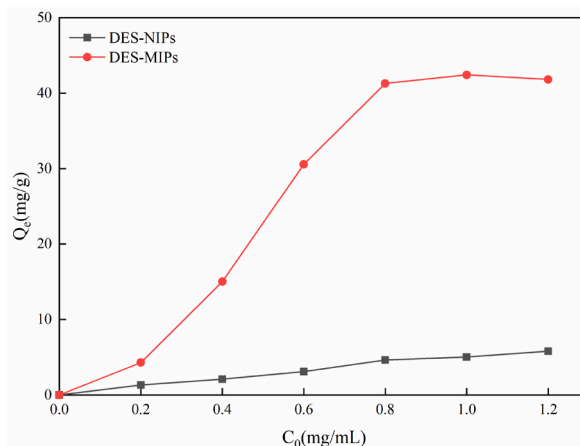


Fig. 7. Adsorption isotherm curve of DES-MIPs and DES-NIPs.

of Freundlich. K_L and K_F are the equilibrium constants for Langmuir and Freundlich adsorption processes, respectively.

For DES-MIPs, the Langmuir fitting correlation coefficient $R^2 = 0.98073$ and Freundlich fitting correlation coefficient $R^2 = 0.96743$, demonstrating that Langmuir model is applicable to the adsorption of HT by MIPs. For DES-NIPs, the Langmuir fitting correlation coefficient $R^2 = 0.98763$ and Freundlich fitting correlation coefficient $R^2 = 0.98646$, indicating that Langmuir model and Freundlich are suitable for the adsorption of HT on DES-NIPs. Adsorption isothermal model parameters were shown in Table S4.

3.3.4. Selectivity test

In the selectivity experiment, Oleuropein and Syringin were chosen as the competing compounds of HT to explore and analyze the selectivity of DES-MIPs. The contents of HT, Oleuropein and Syringin in DES-MIPs and DES-NIPs residual solution were determined by HPLC. The adsorption capacities of HT and competitors on DES-MIPs were shown in Fig. 8(a). The adsorption capacity of DES-MIPs was confirmed to be higher than that of DES-NIPs. Furthermore, DES-MIPs showed high specific selective adsorption to HT under the competition of these three compounds. The superior recognition of HT by DES-MIPs was related to the size, shape and special functional groups of HT at the specific imprinting sites. In conclusion, the number of blot sites of DES-MIPs for Oleuropein and Syringin were lower than HT, indicating that the selectivity and affinity of DES-MIPs for HT was higher than that of its competitors. The adsorption capacity of DES-NIPs on HT was similar with Oleuropein and Syringin, proving that there was no special memory site on DES-NIPs. Moreover, the adsorption capacity of HT was the highest (41.39 mg/g) among these three compounds, demonstrating that DES-MIPs possessed the highest selective capacity for HT. This result suggested that DES-MIPs showed stronger pore characteristics and specific recognition for HT than the other two compounds, while DES-NIPs showed almost no specificity for these three compounds.

3.4. Reusability test of DES-MIPs

Reusability and stability of DES-MIPs were investigated, and possibility and value of DES-MIPs in practical application were further evaluated. HT was eluted with methanol-acetic acid (9:1, v/v) as the eluting solvent (The selecting of the elution solvent is given by Table S2). The adsorption/desorption cycle was performed 5 times. Fig. 8(b) showed the adsorption capacity percentage of DES-MIPs. After three cycles, the adsorption capacity of DES-MIPs was much more than 85 % of the initial adsorption capacity, and after the fifth cycle, the adsorption capacity of DES-MIPs was 80.50 % of the initial adsorption capacity. After repeated adsorption/desorption experiments, DES-MIPs still has outstanding adsorption performance, proving that DES-MIPs has good reusability and stability.

4. Conclusions

In our work, a novelty and utility DES-MIPs were produced to Special recognize and separate HT. $\text{Fe}_3\text{O}_4@\text{SiO}_2@\text{VTEOs}$ was successfully used as the matrix to prepare the magnetic core-shell nanoparticles with DES as the functional monomer. The magnetic Fe_3O_4 was used as the matrix to realize rapid separation. The DES was regarded as a simple and convenient synthesis material as a functional monomer with affordable, easily prepared and nontoxicity. The synthesized DES-MIPs were characterized by SEM, TEM, DLS, FT-IR, XRD, TGA and VSM, which confirmed that DES-MIPs had been successfully synthesized and had good thermal stability and magnetism. Compared with magnetic DES-NIPs ($Q = 4.64 \text{ mg g}^{-1}$), DES-MIPs nanoparticles have excellent adsorption capacity ($Q = 42.43 \text{ mg g}^{-1}$). The optimal reaction concentration of HT is 1.00 mg/mL, and the adsorption process conforms to the Langmuir model ($R^2 = 0.98073$). According to the comparison of adsorption performance, 140 μL of DES ($Q = 42.23 \text{ mg g}^{-1}$) was selected as the optimal number of DES-MIPs. The adsorption process can reach saturated adsorption in 300 min, and the adsorption process conforms to the Pseudo-first-order model ($R^2 = 0.98623$). In the selectivity experiment, the adsorption capacity of DES-MIPs for HT was 40.11

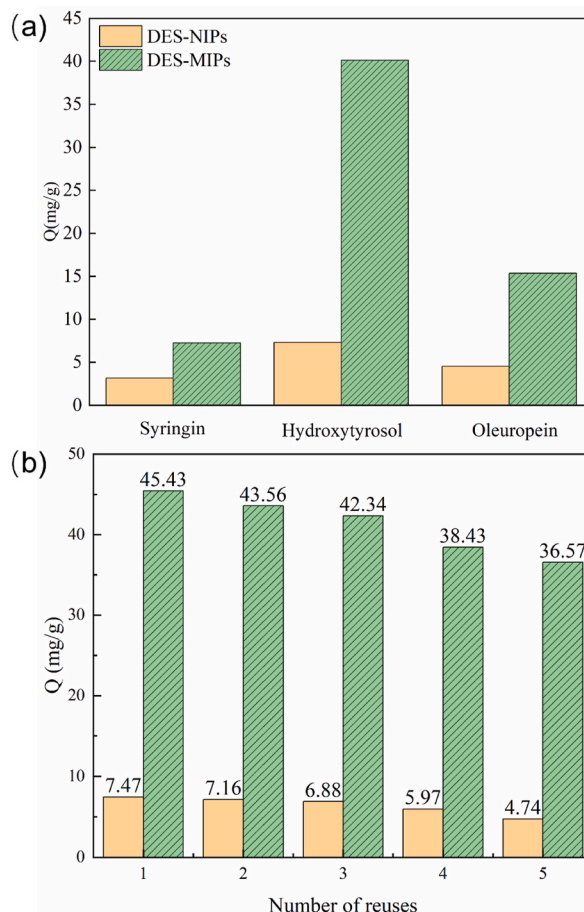


Fig. 8. Selectivity test (a), adsorption-desorption cycles (b) of DES-MIPs and DES-NIPs.

mg g^{-1} , and for Syringin and Oleuropein was 7.24 and 15.35 mg g^{-1} , showing the specific adsorption capacity of DES-MIPs.

Data availability

Data will be made available on request.

CRediT authorship contribution statement

Xiaojing Wang: Writing – original draft, Conceptualization. **Mengru Wang:** Writing – review & editing. **Bailin Wu:** Investigation. **Shengyuan Yu:** Investigation. **Zaizhi Liu:** Formal analysis. **Xuyang Qin:** Formal analysis. **Huijuan Xu:** Writing – review & editing, Visualization. **Wei Li:** Methodology. **Sha Luo:** Data curation. **Lijuan Wang:** Resources. **Chunhui Ma:** Resources, Project administration, Funding acquisition, Conceptualization. **Shouxin Liu:** Supervision.

Declaration of competing interest

The authors declare that they have no known competing financial interests or personal relationships that could have appeared to influence the work reported in this paper.

Acknowledgement

This work was financially supported by the Fundamental Research Funds for the Central Universities (2572022BB06), and the National Undergraduate Training Programs for Innovations (202110225022).

Appendix ASupplementary data

Supplementary data to this article can be found online at <https://doi.org/10.1016/j.heliyon.2024.e28257>.

References

- [1] A. Dobrinčić, M. Repajić, I.E. Garofulić, L. Tuden, V. Dragović-Uzelac, B. Levaj, Comparison of different extraction methods for the recovery of olive leaves Polyphenols, *Processes* 8 (2020) 1008, <https://doi.org/10.3390/pr8091008>.
- [2] M. Costa, S. Losada-Barreiro, C. Bravo-Díaz, L.S. Monteiro, F. Paiva-Martins, Interfacial concentrations of hydroxytyrosol derivatives in fish oil-in-water emulsions and nanoemulsions and its influence on their lipid oxidation: droplet size effects, *Foods* 9 (2020) 1897, <https://doi.org/10.3390/foods9121897>.
- [3] A. Bermúdez-Oria, G. Rodríguez-Gutiérrez, F. Rubio-Senent, Á. Fernández-Prior, J. Fernández-Bolaños, Effect of edible pectin-fish gelatin films containing the olive antioxidants hydroxytyrosol and 3,4-dihydroxyphenylglycol on beef meat during refrigerated storage, *Meat Sci.* 148 (2019) 213–218, <https://doi.org/10.1016/j.meatsci.2018.07.003>.
- [4] A. Mosca, A. Crudele, G. Tozzi, T. Alterio, A. Smeriglio, D. Trombetta, A. Alisi, The anti-inflammatory effects of hydroxytyrosol and vitamin e on paediatric NAFLD, *Dig. Liver Dis.* 52 (2020) 42–43, <https://doi.org/10.1016/j.dld.2019.12.138>.
- [5] R. Hornedo-Ortega, A.M. Espinosa-Oliva, Evidences of hydroxytyrosol as an anti-inflammatory agent in Parkinson's disease: insights into the mechanisms of action, *Neural Regener. Res.* 16 (2021) 992–993, [10.4103/1674-5374.297075](https://doi.org/10.4103/1674-5374.297075).
- [6] M. Centrone, M. D'Agostino, G. Difonzo, A. De Bruno, A. Di Mise, M. Ranieri, G. Tamma, Antioxidant efficacy of olive by-product extracts in human colon HCT8 Cells, *Foods* 10 (2021) 11, <https://doi.org/10.3390/foods10010011>.
- [7] J. Icamí, L.M. Bedoya, P. Obregón, M. Beltrán, E. Gomez-Acebo, D. Auñón, L. Capa, Antiviral activity of 5-hydroxytyrosol, a microbicidal candidate against HIV-1 transmission, *AIDS Res. Hum. Retrovir.* 30 (2014) 240, <https://doi.org/10.1089/aid.2014.5531.abstract>.
- [8] M. Safi, H. Onori, M. Rahmati, Investigation of the anti-cancer effects of free and PLGA-PAA encapsulated hydroxytyrosol on the MCF-7 breast cancer cell line, *Curr. Mol. Med.* 22 (2022) 657–662, <https://doi.org/10.2174/1566524020666201231103826>.
- [9] S. Zhang, J. Zhou, Q. Fan, X. Lv, T. Wang, F. Wang, Y. Zhang, Discovery of hydroxytyrosol as thioredoxin reductase 1 inhibitor to induce apoptosis and G(1)/S cell cycle arrest in human colorectal cancer cells via ROS generation, *Exp. Ther. Med.* 22 (2021) 829, <https://doi.org/10.3892/etm.2021.10261>.
- [10] S. Tejada, S. Pinya, M.D. Biliboni, J.A. Tur, A. Pons, A. Sureda, Cardioprotective effects of the polyphenol hydroxytyrosol from olive oil, *Curr. Drug Targets* 18 (2017) 1477–1486, <https://doi.org/10.2174/1389450117666161005150650>.
- [11] X. Zhang, Y. Qin, X. Wan, H. Liu, C. Iv, W. Ruan, L. Lu, H. Lin, X. Guo, Hydroxytyrosol plays antiatherosclerotic effects through regulating lipid metabolism via inhibiting the p38 signal pathway, *BioMed Res. Int.* 2020 (2020) 5036572, <https://doi.org/10.1155/2020/5036572>.
- [12] F. Costantini, C. Di Sano, G. Barbieri, The hydroxytyrosol induces the death for apoptosis of human melanoma cells, *Int. J. Mol. Sci.* 21 (2020) 8074, <https://doi.org/10.3390/ijms21218074>.
- [13] S. Cetrullo, S. D'Adamo, S. Guidotti, R.M. Borzi, F. Flamigni, Hydroxytyrosol prevents chondrocyte death under oxidative stress by inducing autophagy through sirutin 1-dependent and -independent mechanisms, *Biochim. Biophys. Acta, Gen. Subj.* 1860 (2016) 1181–1191, <https://doi.org/10.1016/j.bbagen.2016.03.002>.
- [14] M. Kafkaletou, G. Ouzounidou, E. Tsantili, Fruit ripening, antioxidants and oil composition in koroneiki olives (*olea europea* L.) at different maturity indices, *Agronomy* 11 (2021) 122, <https://doi.org/10.3390/agronomy11010122>.
- [15] A. Francioso, R. Federico, A. Maggiore, M. Fontana, A. Boffi, M. D'Erme, L. Mosca, Green route for the isolation and purification of hydroxytyrosol, tyrosol, oleacein and oleocanthal from extra virgin olive oil, *Molecules* 25 (2020) 3654, <https://doi.org/10.3390/molecules25163654>.
- [16] M. Dinc, C. Esen, B. Mizaiakoff, Recent advances on core-shell magnetic molecularly imprinted polymers for biomacromolecules, *TrAC, Trends Anal. Chem.* 114 (2019) 202–217, <https://doi.org/10.1016/j.trac.2019.03.008>.
- [17] M.M. Moein, A. Abdel-Rehim, M. Abdel-Rehim, Recent applications of molecularly imprinted sol-gel methodology in sample preparation, *Molecules* 24 (2019) 2889, <https://doi.org/10.3390/molecules24162889>.
- [18] C. Liang, Z. Zhang, H. Zhang, L. Ye, J. He, J. Ou, Q. Wu, Ordered macroporous molecularly imprinted polymers prepared by a surface imprinting method and their applications to the direct extraction of flavonoids from Ginkgo leaves, *Food Chem.* 309 (2020) 125680, <https://doi.org/10.1016/j.foodchem.2019.125680>.
- [19] G.F. Abu-Alsoud, C.S. Bottaro, Porous thin-film molecularly imprinted polymer device for simultaneous determination of phenol, alkylphenol and chlorophenol compounds in water, *Talanta* 223 (2021) 121727, <https://doi.org/10.1016/j.talanta.2020.121727>.
- [20] L. Duan, Y. Zhao, Zwitterionic molecularly imprinted cross-linked micelles for alkaloid recognition in water, *J. Org. Chem.* 84 (2019) 13457–13464, <https://doi.org/10.1021/acs.joc.9b01629>.
- [21] F. Kartal, A. Denizli, Molecularly imprinted cryogel beads for cholesterol removal from milk samples, *Colloids Surf., B* 190 (2020) 110860, <https://doi.org/10.1016/j.colsurfb.2020.110860>.
- [22] J. Chen, Y. Li, X. Wang, W. Liu, Application of deep eutectic solvents in food analysis: a review, *Molecules* 24 (2019) 4594, <https://doi.org/10.3390/molecules24244594>.
- [23] X. Li, K.H. Row, Development of deep eutectic solvents applied in extraction and separation, *J. Separ. Sci.* 39 (2016) 3505–3520, <https://doi.org/10.1002/jssc.201600633>.
- [24] J. Ding, L. Cheng, Core-shell Fe₃O₄@SiO₂@PANI composite: preparation, characterization, and applications in microwave absorption, *J. Alloys Compd.* 881 (2021) 160574, <https://doi.org/10.1016/j.jallcom.2021.160574>.
- [25] Z. Wei, X. Sun, L. Mu, Y. Huang, Z. Liu, Improving affinity of imprinted monolithic polymer prepared in deep eutectic solvent by metallic pivot, *J. Chromatogr., A* 1602 (2019) 48–55, <https://doi.org/10.1016/j.chroma.2019.05.034>.
- [26] W. Zhang, Y. Zhang, R. Wang, P. Zhang, Y. Zhang, E. Randell, P. Zhang, Q. Jia, A review: development and application of surface molecularly imprinted polymers toward amino acids, peptides, and proteins, *Anal. Chim. Acta* 1234 (2022) 340319, <https://doi.org/10.1016/j.aca.2022.340319>.
- [27] Z. Wen, D. Gao, J. Lin, S. Li, K. Zhang, Z. Xia, D. Wang, Magnetic porous cellulose surface-imprinted polymers synthesized with assistance of deep eutectic solvent for specific recognition and purification of bisphenols, *Int. J. Biol. Macromol.* 216 (2022) 374–387, <https://doi.org/10.1016/j.ijbiomac.2022.06.187>.
- [28] E.A. Dil, A.H. Doustimotlagh, H. Javadian, A. Asfaram, M. Ghaedi, Nano-sized Fe₃O₄@SiO₂-molecular imprinted polymer as a sorbent for dispersive solid-phase microextraction of melatonin in the methanolic extract of *Portulaca oleracea*, biological, and water samples, *Talanta* 221 (2021) 121620, <https://doi.org/10.1016/j.talanta.2020.121620>.
- [29] S. Ramanavicius, A. Jagminas, A. Ramanavicius, Advances in molecularly imprinted polymers based affinity sensors, *Polymers* 13 (6) (2021) 974, <https://doi.org/10.3390/polym13060974> (Review).
- [30] Simonas Ramanavicius, Arunas Ramanavicius, Development of molecularly imprinted polymer based phase boundaries for sensors design, *Adv. Colloid Interface Sci.* 305 (2022) 102693, <https://doi.org/10.1016/j.cis.2022.102693> (review).
- [31] X. Li, K. Row, Purification of antibiotics from the millet extract using hybrid molecularly imprinted polymers based on deep eutectic solvents, *RSC Adv.* 7 (2017) 16997–17004, <https://doi.org/10.1039/c7ra01059a>.
- [32] X. Zhang, Y. Wang, Z. Wei, D. An, W. Pu, Z. Liu, Y. Huang, Improving the identification of lysine-acetylated peptides using a molecularly imprinted monolith prepared by a deep eutectic solvent monomer, *J. Proteome Res.* 21 (2020) 325–338, <https://doi.org/10.1021/acs.jproteome.1c00553>.

- [33] M. Chai, X. Zhang, L. Zhao, W. Hao, Y. Huang, Z. Liu, Combination of deep eutectic solvent and organic-inorganic hybrid monomer to prepare monolith for improvement of hydrophilic protein extraction, *Microchem. J.* 177 (2022) 107310, <https://doi.org/10.1016/j.microc.2022.107310>.
- [34] Prof A.P. Abbott, G. Capper, S. Gray, Design of improved deep eutectic solvents using hole theory, *ChemPhysChem* 7 (2006) 803–806, <https://doi.org/10.1002/cphc.200500489>.
- [35] Y. Ji, J. Zhao, L. Zhao, Fabrication and characterization of magnetic molecularly imprinted polymer based on deep eutectic solvent for specific recognition and quantification of vanillin in infant complementary food, *Food Chem.* 374 (2020) 131720, <https://doi.org/10.1016/j.foodchem.2021.131720>.
- [36] Baskar Thangaraj, Zhaohua Jia, Lingmei Dai, Dehua Liu, Wei Du, Effect of silica coating on Fe₃O₄ magnetic nanoparticles for lipase immobilization and their application for biodiesel production, *Arab. J. Chem.* 12 (2019) 4694–4706, <https://doi.org/10.1016/j.arabjc.2016.09.004>.
- [37] Wei Xu, Yuzhi Wang, Xiaoxiao Wei, Jing Chen, Panli Xu, Rui Ni, Jiaojiao Meng, Yigang Zhou, Fabrication of magnetic polymers based on deep eutectic solvent for separation of bovine hemoglobin via molecular imprinting technology, *Anal. Chim. Acta* 1048 (2019) 1–11, <https://doi.org/10.1016/j.aca.2018.10.044>.
- [38] Ziwei Liu, Yuzhi Wang, Fangting Xu, Xiaoxiao Wei, Jing Chen, Heqiong Li, Xiyan He, Yigang Zhou, A new magnetic molecularly imprinted polymer based on deep eutectic solvents as functional monomer and cross-linker for specific recognition of bovine hemoglobin, *Anal. Chim. Acta* 1129 (2020) 49–59, <https://doi.org/10.1016/j.aca.2020.06.052>.
- [39] Adrián Gutiérrez-Serpa, Raúl González-Martín, Muhammad Sajid, Verónica Pino, Greenness of magnetic nanomaterials in miniaturized extraction techniques: a review, *Talanta* 225 (2021) 122053, <https://doi.org/10.1016/j.talanta.2020.122053>.